Genetic, functional, and structural implications of *TMEM175* variants in Parkinson disease and REM sleep behavior disorder

Lynne Krohn, BSc[1,2,*], Tuğba Nur Öztürk, MSc[3,5,6,7,*], Benoit Vanderperre, PhD[4,*], Jennifer A. Ruskey, MSc[2,8], Sandra B. Laurent,[2,8], Dan Spiegelman, MSc[2,8], Ronald B. Postuma, MD[2,8,29], Isabelle Arnulf, PhD, MD[9], Michele T.M. Hu, PhD, FRCP[10,11], Yves Dauvilliers, PhD, MD[12], Birgit Högl, MD[13], Ambra Stefani, MD[13], Christelle Charley Monaca, MD[14], Giuseppe Plazzi, MD[15,16], Elena Antelmi, PhD[15,16], Luigi Ferini-Strambi, MD[17], Anna Heidbreder, MD[18], Valérie Cochen De Cock, MD[19,20], Peter Young, MD[18], Pavlina Wolf, BSc,[21] Petra Oliva, PhD,[21] Xiaokui Kate Zhang, PhD,[21,] Lior Greenbaum, PhD[22], Christopher Liong, BA,[23], Jean-François Gagnon, PhD[24,25], Alex Desautels, PhD, MD[8], Sharon Hassin-Baer, MD[22], Jacques Y. Montplaisir, PhD, MD[24,26], Nicolas Dupré, MD, FRCP[27,28], Guy A. Rouleau PhD, MD, FRCPC, FRSC[1,2,8], Jean Francois Trempe, PhD[29], Guillame Lamoureaux, PhD[3,5,6,7,30,], Edward A. Fon, MD[2,4], Roy N. Alcalay, MD, MS[23,31], Ziv Gan-Or, PhD, MD[1,2,8].

Affiliations

1.Department of Human Genetics, McGill University, Montréal, QC, Canada. 2. Montreal Neurological Institute, McGill University, Montréal, QC, Canada. 3. Department of Physics, Concordia University, Montréal, QC, Canada. 4. Department of Experimental Medicine, McGill University, Montréal, QC, Canada. 5. Centre for Research in Molecular Modeling (CERMM), Concordia University, Montréal, QC, Canada. 6. Groupe d'étude des protéines membranaires (GÉPROM). 7. PROTEO, The Québec Network for Research on Protein Function, Engineering and Applications, Québec, QC, Canada. 8. Department of Neurology and Neurosurgery, McGill University, Montréal, QC, Canada. 9. Sleep Disorders Unit, Pitié Salpêtrière Hospital, Centre de Recherche de l'Institut du Cerveau et de la Moelle Epinière and Sorbonne Universities, Paris, France. 10. Oxford Parkinson's Disease Centre (OPDC), University of Oxford, Oxford, United Kingdom. 11. Nuffield Department of Clinical Neurosciences, University of Oxford, Oxford, United Kingdom. 12. National Reference Center for Narcolepsy, Sleep Unit, Department of Neurology, Gui-de-Chauliac Hospital, CHU Montpellier, University of Montpellier, Inserm U1061, Montpellier, France. 13. Sleep Disorders Clinic, Department of Neurology, Medical University of Innsbruck, Innsbruck, Austria. 14. University Lille North of France, Department of Clinical Neurophysiology and Sleep Center, CHU Lille, Lille, France. 15. Department of Biomedical and Neuromotor Sciences (DIBINEM), Alma Mater Studiorum, University of Bologna, Bologna, Italy. 16. IRCCS, Institute of Neurological Sciences of Bologna, Bologna, Italy. 17. Department of Neurological Sciences, Università Vita-Salute San Raffaele, Milan, Italy. 18. Department of Sleep Medicine and Neuromuscular Disorders, University of Muenster, Germany. 19. Sleep and Neurology Unit, Beau Soleil Clinic, Montpellier, France. 20. EuroMov, University of Montpellier, Montpellier, France. 21. Biologics Structural and Functional Research, Biopharmaceutics Development, Genzyme, a Sanofi company, Framingham, MA, USA. 22. Department of Neurology and Sagol Neuroscience Center, Chaim Sheba Medical Center, The Movement Disorders Institute, Tel-Hashomer, Ramat Gan, Israel. 23. Department of Neurology, College of Physicians and Surgeons, Columbia University Medical Center, New York, NY, USA. 24. Centre d'Études Avancées en Médecine du Sommeil, Hôpital du Sacré-Cœur de Montréal, Montréal, QC, Canada. 25. Département de Psychologie, Université du Québec à Montréal, Montréal, QC, Canada. 26. Department of Psychiatry, Université de Montréal, Montréal, QC, Canada. 27. Division of Neurosciences, CHU de Québec, Université Laval, Québec City, QC, Canada; 28. Department of Medicine, Faculty of Medicine, Université Laval, Québec City, QC, Canada. 29. Department of Pharmacology & Therapeutics, McGill University, Montréal, Québec, Canada. 30. Department of Chemistry and Biochemistry, Concordia University, Montréal, Canada. 31. Taub Institute for Research on Alzheimer's Disease and the Aging Brain, College of Physicians and Surgeons, Columbia University Medical Center, New York, NY, USA.

[*] Equal contribution

Corresponding author:
Ziv Gan-Or

Montreal Neurological Institute,
McGill University
1033 Pine Avenue, West,
Ludmer Pavilion, room 312
Montreal, QC, H3A 1A1,
Phone: +1-514-398-5845
e-mail: ziv.gan-or@mcgill.ca

Running title: *TMEM175* in PD and RBD

Characters
Title: 106
Running head: 21

Words
Abstract: 250
Introduction:
Discussion:

Body:

Tables & Figures
Tables: 1
Figures: 7
Supplementary Tables: 2

The final article is available at: Krohn, L., Öztürk, T. N., Vanderperre, B., Ouled Amar Bencheikh, B., Ruskey, J. A., Laurent, S. B., Spiegelman, D., Postuma, R. B., Arnulf, I., Hu, M. T. M., Dauvilliers, Y., Högl, B., Stefani, A., Monaca, C. C., Plazzi, G., Antelmi, E., Ferini-Strambi, L., Heidbreder, A., Rudakou, U., Cochen De Cock, V., … Gan-Or, Z. (2020). Genetic, Structural, and Functional Evidence Link TMEM175 to Synucleinopathies. *Annals of Neurology, 87*(1), 139–153. https://doi.org/10.1002/ana.25629

Abstract

Objective: The *TMEM175/GAK/DGKQ* locus is the 3rd strongest risk locus in genome-wide association studies (GWAS) of Parkinson disease (PD). We aimed to identify the specific disease-associated variants in this locus, and their potential implications.

Methods: Full sequencing of *TMEM175/GAK/DGKQ,* followed by genotyping of specific associated variants was performed in PD (n=1,575) and rapid eye movement (REM)-sleep behavior disorder (RBD) patients (n=533) and in controls (n=1,583). Adjusted regression models and a meta-analysis were performed. Association between variants and glucocerebrosidase (GCase) activity was analyzed in 715 individuals with available data. Homology modelling and molecular dynamics simulations were performed on *TMEM175* variants to determine their potential effects on structure and function. CRISPR knockout of TMEM175 was performed in HeLa cells, and accumulation of α-synuclein was measured.

Results: Two coding variants, *TMEM175* p.M393T (OR=1.37, *p*=0.0003) and p.Q65P (OR=0.72, *p*=0.005) were associated with PD, and p.M393T was also associated with RBD (OR=1.59, *p*=0.001). *TMEM175* p.M393T was associated with reduced GCase activity. Homology modelling and molecular dynamics simulations demonstrated that *TMEM175* p.M393T creates a polar side-chain in the hydrophobic core of the transmembrane, which could destabilize the domain and thus impair either its assembly, maturation, or trafficking. The p.Q65P variant may lead to better stability and performance of the transmembrane protein. Lastly, *TMEM175* knockout resulted in ~4-fold increase in α-synuclein levels in HeLa cells.

Interpretation: Our results demonstrate that coding variants in *TMEM175* are responsible for the association in the *TMEM175/GAK/DGKQ* locus, and suggest that this may be mediated by affecting GCase activity and α-synuclein accumulation.

Introduction

In recent years, genome wide association studies (GWAS) in Parkinson disease (PD) have provided us with a wealth of information on the genetic factors underlying the risk for PD.[1, 2] However, for most of the GWAS loci, the exact genetic cause within each locus is still unknow. The *TMEM175/GAK/DGKQ* locus is the third most significant peak in two large meta-analyses of PD risk genome-wide association studies (GWAS).[1, 2] It is still not certain which of the three genes is the primarily responsible for the risk association, although initial findings suggested that coding variants in *TMEM175* may be linked to PD and responsible for the association in this locus.[2] Interestingly, the *TMEM175* p.M393T variant is one of few coding variants to be the most significant marker in a PD risk locus.

TMEM175 encodes for a transmembrane organelle potassium channel which was shown to regulate lysosomal function.[3] The autophagy lysosomal pathway (ALP) likely plays a large role in Parkinson disease (PD) pathogenesis[4], as deficits in the ALP may lead to alpha-synuclein protein aggregation and accumulation and reduction in glucocerebrosidase (GCase) activity[5]. GCase is encoded by *GBA*, which harbors variants that are among the most common risk factors for PD.[2, 6, 7] Although information is recent and still incomplete about the function of TMEM175, it was shown that lysosomes lacking TMEM175 have reduced potassium conductance and compromised luminal pH stability, resulting in abnormal fusion with autophagosomes during autophagy.[8] Furthermore, studies in cellular models demonstrated that TMEM175 knockdown also resulted in reduced activity of GCase.[8]

In the current study, we aimed to further examine the *TMEM175/GAK/DGKQ* PD risk locus in PD, as well as rapid eye movement (REM) sleep behavior disorder (RBD). Most individuals with RBD in fact have prodromal synucleinopathy, and >80% of them are likely to

progress to PD, dementia with Lewy bodies (DLB) or multiple system atrophy (MSA).[9] Furthermore, RBD may be a clinical marker for specific PD subtype,[10] and only in recent years genetic studies of RBD have been emerged. To study this locus in PD and RBD, we performed targeted next generation sequencing of the coding and regulatory regions of *TMEM175, GAK,* and *DGKQ*, followed by genotyping of two *TMEM175* coding variants in three PD and one RBD cohorts. In addition, we analyzed the structural impact of the two *TMEM175* risk variants, the effects of *TMEM175* knock-out on α-synuclein, and the association between deleterious *TMEM175* variant p.M393T with GCase activity in PD patients.

Methods

Population

First, *TMEM175, GAK* and *DGKQ* were sequenced in a discovery cohort of unrelated, consecutively recruited PD patients (n=586), idiopathic RBD patients (n=350) and controls (n=869) of European ancestry (confirmed for all cases and controls using HapMap v.3 in hg19/GRCh37 and principal component analysis). Based on the results from the discovery cohort, the analysis of specific *TMEM175* variants was expanded to include three PD cohorts (n=1,575), an expanded RBD cohort (n=533) and controls (n=1,583). A cohort from Columbia University included 482 PD patients (average age at enrollment 66±11, 69% men) and 233 controls (65±10 years, 35% men). A cohort from Sheba medical center included 450 PD patients (62±12, 64% men) and 432 young controls (34±7, 60% men) of Ashkenazi Jewish origin. The young controls represent the general Ashkenazi Jewish population, and composed of individuals who performed routine genetic testing in Sheba medical center. A cohort collected at McGill University through numerous collaborators included 641 PD patients (66±10, 66% men), 533 RBD patients (68±9,

80% men) and 910 controls (43±14, 51% men). These 910 controls were composed of elderly controls (n=225, 63.5±8 years) and young controls (n=650, 36±7, additional 35 controls with no data on age). Since the analyzed variant frequencies were similar in these two control groups, we could combine them for the analysis. All differences in sex and age were taken into account and adjusted for in the statistical analysis. PD was diagnosed by movement disorder specialists according to the UK Brain Bank Criteria[11] without excluding patients who have relatives with PD. Study protocols were approved by the Institutional Review Board and all patients signed informed consent before participating in the study.

Genetic analysis

DNA was extracted using a standard salting out protocol. In the discovery cohort, the coding and regulatory regions of *TMEM175, GAK,* and *DGKQ* were targeted with Molecular Inversion Probes (MIPs) designed as previously described, [12] and the targeting probes are detailed in Table S1. Targeted DNA capture and amplification was done as previously described,[13] and the full protocol is available upon request. The MIPs library was sequenced using Illumina HiSeq 2500 platform at the McGill University and Genome Quebec Innovation Centre. Sequence processing was done by Burrows-Wheeler Aligner for alignment[14], the Genome Analysis Toolkit (GATK, v3.8)[15] for post-alignment cleanup and variant calling, and ANNOVAR for annotation[16]. Variant frequencies were extracted from the public database Exome Aggregation Consortium (ExAC)[17] and PDgene.[18] Following the discovery phase, specific TaqMan probes (Thermo Fisher Scientific Inc.) were used to genotype *TMEM175* p.M393T (rs34311866, assay# C__25756279_10) and p.Q65P (rs34884217, assay# C__25751669_10) according to the manufacturer instructions. Genotyping was done on a QuantStudio™ 7 Flex and analyzed with QuantStudio™ Real-time PCR software

v. 1.3. TaqMan genotyping results confirmed the MIP calls at 15X coverage, and if a discrepancy was found, the sample was removed from the analysis.

GCase activity

Measurement of GCase activity was performed at Sanofi laboratories, and the researchers were blinded to the genetic status of the samples. Dried blood spots were obtained using previously published protocols[19, 20] in the NY cohort. Gcase activity was measured using a previously published protocol as part of a multiplex assay together with four additional lysosomal enzymes.[21] All analyses were monitored on an API 4000 triple quadrupole mass spectrometer (ABSciex, Framingham, Massachusetts, USA) by selected ion monitoring (Multiple Reaction Monitoring, MRM) in positive mode. The enzyme activity of each sample was calculated from the ion abundance ratio of product to internal standard as measured by the mass spectrometer. The background activity of blank filter paper was subtracted from the dried blood spot activity. Two quality-control (QC) samples with previously established activity levels for each enzyme and disease positive samples were included in each plate for QC.

Statistical Analysis

Association of *TMEM175, GAK,* and *DGKQ* variants with PD and RBD was calculated using binary logistic regression, adjusted for age and sex, with case status as the dependent variable. Linear regression was used to test association between *TMEM175* nonsynonymous variant p.M393T and glucocerebrosidase (GCase) activity in the Columbia cohort, adjusting for age, sex, and known GCase influencers *LRRK2* p.G2019S and *GBA* mutations.[21] Association between PD age at onset (AAO) and p.M393T in *GBA* variant carriers was analyzed using ANOVA and linear

regression adjusted for *LRRK2* p.G2019S and severity of *GBA* mutation, both of which affect the AAO.[6] Pooled odds ratios (ORs) and p-values for the PD cohorts were calculated by meta-analysis using R package Metafor[22] in a fixed-effect model. Cochran's *Q*-test was applied to test for residual heterogeneity. All other statistical analyses were performed in either R, SPSS version 21.0 or plink version 1.9.[23]

Homology modelling and molecular dynamics simulations

For the normal mode analysis, homology models of the N- and C-terminal domains were built in SWISS-MODELLER, using the sequence alignment shown in supplementary Fig 1A. The coordinates were submitted to the DynaMut server for analysis.[24] For molecular dynamics, All-atom models of human TMEM175 were constructed with MODELLER,[25] using the crystal structure of *Chamaesiphon minutus* TMEM175 channel[26] (pdb 5VRE) as a template. For the chain A and chain B, residues 36-230 and 261-473 were aligned using LOMETS[27], which returns 10 pairwise alignments, which we combined into a single alignment for which no gaps were introduced in alpha-helices (Fig 1A). Protein models were generated from residues 21 to 477 for both chains and the N and C termini were neutralized (acetylated and amidated, respectively). Residue His57 was protonated ("HSP 57") to account for the low pH extracellular environment. Models were oriented using the OPM database[28] (5VRE entry) and, using CHARMM-GUI[29], were embedded in a hydrated 1-palmitoyl-2-oleoyl-phosphatidylcholine (POPC) bilayer with 150mM KCl to obtain a simulation cell of dimensions 97 × 97 × 134 Å. The simulation system consisted of ~117,300 atoms. CHARMM36[30] force field and TIP3P water model were used. All simulations were equilibrated using the six-step scheme suggested by Jo and coworkers[31] by doubling the equilibration time in the first three steps (50 ps each). The production steps were performed in the

NPT ensemble (310 K and 1 atm) using NAMD 2.9[32] with a 2 fs timestep. Following these six equilibration steps, the dihedral angles of residues 37 to 54 and 265 to 279 (forming the ion pore) were restrained for the first 10 ns of production, with a force constant of 500 kcal/mol/rad[25]. Temperature and pressure were kept constant using Langevin dynamics with a coupling coefficient of 1 ps^{-1} and using a Nosé-Hoover Langevin piston,[33, 34] with a piston period of 50 fs and a piston decay of 25 fs. All bonds involving hydrogen atoms were constrained using the SHAKE/RATTLE[35] algorithm. Nonbonded interactions were calculated using particle mesh Ewald[36] and the recommended CHARMM cutoff scheme.[37] Five independent initial structures were generated for each channel (WT and Q65P mutant) and 100 ns long production simulations were performed for all of them. The last 90 ns of each trajectory were analyzed, for a total of 450 ns for WT and Q65P channels.

Cell culture and TMEM175 knock-out in Hela cells using CRISPR/Cas9

HeLa cells were obtained from ATCC, maintained at 37°C and 5% CO2 and cultured in Dulbecco's modified Eagle medium (DMEM, Wisent Inc.) containing sodium pyruvate, supplemented with 10% heat-inactivated fetal bovine serum (FBS), 2 mM glutamine and 100 units/ml penicillin (Wisent Inc.). To generate TMEM175 knock-out Hela cells, two guide RNAs, sg1 and sg2, were cloned into the pSpCas9(BB)-2A-Puro vector (pX459_v2, Addgene 62988) according to the Zhang lab protocol. Target sequences were (cut site is shown as "*", PAM sequence is in parentheses): sg1 GTCCATCATCGCCACCG*TCA (TGG); sg2 GCAGGCACTGGATACAC*CGG (GGG). jetPRIME transfection reagent was used to co-transfect Hela cells with sg1 and sg2 encoding plasmids according to the manufacturer's protocol (Polyplus transfection). 24 h later, transfected cells were selected with 3 μg/ml puromycin for 48

h. Individual cells were then seeded in 96 wells plates by FACS, and the clones obtained were screened by PCR for loss of a gene fragment (due to cutting at both target sites) and Western blotting.

Immunoblotting

Cells were lysed in Laemmli buffer containing DTT, sonicated and boiled for 10 min before SDS-PAGE and transfer onto a nitrocellulose membrane. For α-synuclein, the membrane was fixed in phosphate-buffered saline (PBS) containing 0.4% paraformaldehyde (PFA) for 30 min as described previously[38]. Membranes were blocked with 5% skim milk in 0.1% Tween-20/PBS (PBS-T) and incubated overnight at 4 °C with primary antibodies in PBS-T containing 1% milk. Primary antibodies were rabbit polyclonal anti-TMEM175 antibody (19925-1-AP, Proteintech, 1:1000), mouse anti-α-synuclein (clone 42/α-Synuclein, BD Transduction Laboratories, 1:1000), or goat anti-GAPDH (NB300-320, Novus Biologicals, 1:20000). Membranes were washed with PBS-T containing 1% milk three times for 5 min and then incubated with a secondary antibody, horseradish peroxidase-conjugated anti-mouse IgG, anti-rabbit IgG or anti-goat IgG antibody (Jackson) at a 1:5000 dilution in PBS-T containing 1% milk for 1 hour at room temperature. Membranes were then washed three times with PBST and developed using ECL substrate (PerkinElmer Life Sciences) on a Bio-Rad ChemiDoc imaging system. Densitometric quantification was performed using ImageJ.

Results

TMEM175 coding variants are associated with risk for PD and RBD.

The average coverage of *TMEM175* was 318X with > 90% of nucleotides with >20X, the average coverage of *GAK* was 371X with > 96% of nucleotides with >20X, and the average coverage of *DGKQ* was 178X with > 88% of nucleotides with >20X. After applying a genotype cut-off of 80% for samples and variants, coverage depth of >15X and removing variants with Hardy-Weinberg equilibrium $p<0.001$, a total of 295 coding variants in PD and 191 in RBD were detected in *GAK, TMEM175*, and *DGKQ* (Table S2). None of the coding variants in *GAK* or *DGKQ* were associated with risk of PD or RBD. Burden analysis using the optimized sequence Kernel association test (SKAT-O) did not identify a significant burden of multiple rare variants in any of the three genes. The nonsynonymous *TMEM175* p.M393T variant was associated with increased risk for both PD (meta-analysis OR=1.37, 95% CI 1.15-1.61, p=0.0003, Table 1, Fig 2) and RBD (OR=1.59, 95% CI 1.20-2.11, p=0.001). In a meta-analysis including the PD and RBD cohorts the OR was 1.42 (95% CI 1.23-1.64, $p<0.0001$, Fig 2). The nonsynonymous *TMEM175* p.Q65P variant was associated with a decreased risk for PD (meta-analysis OR=0.72, 95% CI 0.57-0.91, p=0.005), but not with RBD, despite similar directionality of effect (OR=0.88, 95% CI 0.63-1.23, p=0.45). A meta-analysis combining both PD and RBD had an OR of 0.77 (95% CI 0.63-0.93, p=0.0063, Fig. 2). In all meta-analyses, the heterogeneity test had a $p>0.68$ with and without including RBD, supporting the validity of these models. The variant frequencies and odds ratios for both variants in the PD cohorts were similar with previous results detailed on PDgene (www.pdgene.org, p.M393T OR=1.26, 95%CI 1.22-1.31, $p<5\times10^{-8}$, p.Q65P OR=0.74, 95% CI 0.69-0.81, $p<5\times10^{-8}$).

***TMEM175* p.M393T is associated with reduced GCase activity, and may affect the AAO of *GBA* variant carriers.**

Since *TMEM175* encodes a lysosomal transmembrane channel that was previously suggested to affect GCase activity in cell models,[8] we set to examine whether the risk variants in *TMEM175* may affect GCase activity in humans. Data on GCase activity was available for the NY cohort, and since *GBA* variants and the *LRRK2* p.G2019S mutations also affect GCase activity,[21] they were included as covariates in the model. The p.Q65P variant did not significantly affect GCase activity, however, the p.M393T was associated with decreased GCase activity (p=0.035, beta=-0.72). Overall, the total contribution of *GBA, LRRK2* and *TMEM175* to the GCase variance, as measured by r^2 in the model, was 0.23.

Due to the effect of *TMEM175* p.M393T on GCase activity, we examined this variant effect on AAO of *GBA*-associated PD across the three PD cohorts (n=236). Interestingly, the average AAO among *GBA* mutation carriers with PD was 59.44 years among non-carriers of p.M393T, compared to 57.59 and 56.95 years among heterozygous and homozygous carriers of p.M393T, respectively. However, the association only showed a trend toward statistical significance (p=0.08, linear regression, adjusted for the severity of the *GBA* mutation and the presence of *LRRK2* p.G2019S).

Structural and molecular dynamics experiments suggest that *TMEM175* variants may affect its structure and function.

To determine the potential structural impact of the p.M393T and p.Q65P mutations, we prepared a homology model of the human TMEM175 using the crystal structure of an ortholog from the bacterium *Chamaesiphon minutus* as a template[26]. HsTMEM175 is characterized by two transmembrane (TM) domains in tandem, each showing sequence homology to the single TM domain of CmTMEM175 (Fig 1A, 1B). Since CmTMEM175 forms a K+ channel as a tetramer[26],

HsTMEM175 can adopt two possible pseudo-tetrameric configurations where the two N-terminal domains are either on adjacent or opposite sides (Fig 3). However, the former configuration is unlikely to occur, as its topologies would imply that the linker between the two domains would cross-over the entrance of the channel on the cytoslic side. Thus, two chains of human TMEM175 assemble into a pseudo-tetramer, with the first TM helix from each domain forming the ion conducting pore (Fig 1C, D). Met393 is located in TM4 and its side-chain faces inside the TM domain (Fig 1E). The p.M393T mutation would cause a mild steric clash with an adjacent side-chain, but would also introduce a polar side-chain in the hydrophobic core of the domain, which could destabilize the domain and thus impair either its assembly, maturation, or trafficking.

On the other hand, the protective variant p.Q65P occurs in a loop located after a short helix on the lumenal side of the domain (Fig 1F). This loop contains Glu59, an acidic residue at the entrance of the channel that, together with Asp279 and Glu282, might contribute to ion selectivity. Normal mode analysis of the mutation p.Q65P induces a minor global destabilization ($\Delta\Delta G$: -0.315 kcal/mol) and a local rigidification around the mutation site (Fig 4). However, it is unclear how the backone conformation and ion selectivity would be affected. To address this, we have performed a molecular dynamics (MD) simulation on both the WT and p.Q65P variants for a total of 450 nsec. The simulation was performed in a standard POPC membrane in the presence of K+ ions and water molecules on either side of the membrane. Near the mutation site, one noticeable feature of the simulation is the smaller range of backbone dihedral angles adopted by the p.Q65P variant (Fig 5A). Inspection of MD trajectories shows that the backbone angles of a.a. Gln64/Gln65 undergo "flips" between different allowed configurations (Fig 5B). These flips occured more frequently in the WT than in the p.Q65P variant (Fig 5B). An emergent property from the simulation is that K+ ions reach deeper into the channel in the p.Q65P variant (Fig 5C,D). This could be a consequence

of the p.Q65P variant showing more backbone rigidity, thus presenting ion-guiding side-chains in a more concerted fashion (Fig 6).

TMEM175 deficiency leads to α-synuclein accumulation in cell model.

TMEM175 deficiency has previously been proposed to lead to increased α-synuclein aggregation through decreased autophagic levels in rat primary hippocampal neurons[8]. To study whether TMEM175 is associated with α-synuclein pathology in human cells, we generated *TMEM175* knock-out Hela cells using CRISPR/Cas9. Western blot confirmed the complete loss of all TMEM175-antibody reactive bands in two distinct KO clones (KO-1 and KO-2, Fig 7A), and this was accompanied by a robust and significant ~4-fold increase in endogenous α-synuclein levels (Fig 7A, B), possibly due to decreased lysosomal activity.

Discussion

Our results suggest that within the *TMEM175/GAK/DGKQ* locus, the coding *TMEM175* variants p.M393T and p.Q65P may be responsible for the genetic association with PD risk at this locus. Furthermore, we show that the *TMEM175* p.M393T variant is also associated with risk for idiopathic RBD, and that it is associated with reduced GCase activity. We further provide structural data that may explain how these variants affect the structure and function of the TMEM175 transmembrane channel. As the p.M393T variant may disturb the function of TMEM175, and since it is associated with reduced GCase activity, which is known to be associated with α-synuclein accumulation,[39] we further examined how knockdown of TMEM175 affects α-synuclein levels, and observed an accumulation of α-synuclein in the cell models. These findings support that within this locus, it is *TMEM175* that is associated with risk for PD, potentially by

affecting GCase activity and α-synuclein accumulation. This hypothesis needs to be further explored in follow-up studies.

In the most recent and largest GWAS to date, the index risk variant in the *TMEM175/GAK/DGKQ* region was in strong linkage to the p.M393T variant, associated with an increased PD risk.[1] A secondary hit in the same locus, associated with a reduced PD risk [2], is in linkage with the protective p.Q65P variant (www.pdgene.org). These observations provide further support our findings and conclusions as to the potential role of *TMEM175* in PD. However, we cannot rule out that other, non-coding variants in this locus contribute to PD risk through the involvement of the other genes in this locus. For example, the two reported variants, *TMEM175* p.M393T (rs34311866) and p.Q65P (rs34884217), are strongly associated with differential expression of the *DGKQ* gene in the GTEx database, albeit not in nerve tissues (www.gtexportal.org). Furthermore, it was demonstrated that *GAK* may interact with LRRK2[40], suggesting that this gene may also be involved in PD. Therefore, although the current evidence supporting *TMEM175* as the risk-associated gene in this locus, further studies are required to examine the potential role of *DGKQ* and *GAK* in PD.

Previous genetic studies in RBD suggested that while some of the genes that are associated with PD and DLB, such as *GBA*[41] and the protective *LRRK2* haplotype,[42] are also associated with RBD, other genes such as *MAPT*[43] and *APOE*[44] are not associated with RBD. The current findings demonstrating that the *TMEM175* p.M393T variant is also associated with RBD add to our understanding of the genetic background of RBD. As RBD may represent a specific subtype of synucleinopathies,[10] and since it provides us with a unique opportunity to identify synucleinopathies at a much earlier stage towards future clinical trials,[45] understanding its genetic background and identifying new targets for therapeutics development may be crucial. As an ion

channel, TMEM175 could be highly druggable. Ion channels have long been a focus for therapeutic targets due to their involvement in a wide range of pathologies across all major disease types.[46] Drug treatments targeting membrane proteins are already in use by diseases such as epilepsy, diabetes, and angina, and have established success.[47] As a K+ ion channel with both protective (p.Q65P) and risk increasing (p.M393T) genetic implications in PD, TMEM175 could be a promising target for such therapies, especially if it can be targeted in RBD patients to modify disease course before the major dopaminergic neuron loss seen at the time of PD diagnosis. However, since the function of TMEM175 in the lysosomes is still not completely understood, further functional research is needed.

One of the intriguing findings of the current study is the effect of the *TMEM175* p.M393T risk variant on GCase activity in humans. It has been shown that PD patients both with and without *GBA* mutations show decreased GCase activity[21], suggesting loss of GCase function may contribute to PD pathogenesis. However, the factors that lead to reduced GCase activity in individuals without *GBA* mutation are not known, and the current study suggests that *TMEM175* variants may be one of these factors. This is further supported by previous findings in animal neuronal model where *TMEM175* deficiency was associated with reduced GCase activity.[8] Since we show in the current study that *GBA* mutations, the *LRRK2* p.G2019S mutation and the *TMEM175* p.M393T variant explain only 23% of the variance in GCase activity, it is clear that other genetic or environmental factors also affect GCase activity. Reduction of GCase activity has been shown to increase α-synuclein levels [48], and in the current study we show that *TMEM175* deficiency is associated with α-synuclein accumulation in cell models, as was previously shown in primary rat hippocampal neurons, potentially through its effect on GCase activity.[8] TMEM175 is a potassium ion channel located in late endosomes and lysosomes. It has been shown to regulate

lysosomal membrane potential, pH stability, and organelle fusion via potassium conductance on lysosomal and endosomal membranes[3]. Therefore, the effect on GCase activity in *TMEM175* deficiency could be mediated by the altered lysosomal pH, which is required for proper GCase activity.[8] In addition, reduced GCase activity may increase cell-to-cell transmission of α-synuclein[49], as well as reduce chaperone-mediated autophagy,[48] all potentially contributing to PD pathogenesis. The structural analysis of the two *TMEM175* variants revealed possible mechanisms for involvement in PD pathology. The risk variant p.M393T likely destabilizes the transmembrane domain and thus impairs TMEM175 assembly, maturation, or trafficking. The protective variant p.Q65P potentially increases K+ conductance, thus potentially increasing lysosomal function.

There are several limitations to the current study. First, in the individual PD and RBD cohorts that were used for the genetic analysis, age and sex were not always matched. To address this issue, we adjusted for age and sex in the statistical models, and our results were in line with previous findings in European ancestry cohorts.[1, 2] Notably, there was no significant different between allele frequencies of young and old controls, further allowing us to use younger controls. In addition, although we used the world's largest RBD genetic cohort, power was limited, especially for the protective variant, p.Q65P, which is less common than p.M393T. Of note, there was similar directionality and effect size for the p.Q65P variant in the RBD cohort to that of the PD cohort, albeit not statistically significant. Larger RBD cohort will be required to determine the role of this variant in risk for RBD. Another limitation is the availability of GCase activity only for the NY cohort, and future studies in other cohorts will be required to confirm the association between *TMEM175* variants and GCase activity in humans.

To conclude, the current study together with previous reports, suggest that *TMEM175* coding variants are associated with risk for PD. It further raises the hypothesis that this effect is mediated

by the variants affecting the function of TMEM175, GCase activity and α-synuclein accumulation. These findings highlight *TMEM175* as a potential target for therapeutics development, thus further studies on the function on this gene and transmembrane protein are needed.

Acknowledgements

We thank the patients and control subjects for their participation in this study. This work was financially supported by the Michael J. Fox Foundation, the Canadian Consortium on Neurodegeneration in Aging (CCNA) and the Canadian Glycomics Network (GlycoNet). This research was also undertaken thanks in part to funding from the Canada First Research Excellence Fund (CFREF), awarded to McGill University for the Healthy Brains for Healthy Lives (HBHL) program. The Columbia University cohort is supported by the Parkinson's Foundation, the National Institutes of Health [K02NS080915, and UL1 TR000040] and the Brookdale Foundation. GAR holds a Canada Research Chair in Genetics of the Nervous System and the Wilder Penfield Chair in Neurosciences. ZGO is supported by the Fonds de recherche du Québec - Santé (FRQS) Chercheurs-boursiers award. The access to part of the participants for this research has been made possible thanks to the Quebec Parkinson's Network (http://rpq-qpn.ca/en/). We thank Jay Ross, Daniel Rochefort, Helene Catoire, Cathy Mirarchi and Vessela Zaharieva for their assistance. The Genotype-Tissue Expression (GTEx) Project was supported by the Common Fund of the Office of the Director of the National Institutes of Health, and by NCI, NHGRI, NHLBI, NIDA, NIMH, and NINDS. The data used for the analyses described in this manuscript were obtained from the GTEx Portal on 10/07/18.

Author contributions

Conception and design of the study: LK, TNO, BV, JFT, GL, EAF, RNA, ZG-O

Acquisition and analysis of data: LK, TNO, BV, JAR, SBL, DS, RBP, IA, MTMH, YD, BH, AS, CCM, GP, EA, LF-S, AH, VCDC, PY, PW, PO, XKZ, LG, CL, JFG, AD, SH-B, JYM, ND, GAR, JFT, GL, EAF, RNA, ZG-O

Drafting a significant portion of the manuscript or figures: LK, TNO, BV, JFT, GL, EAF, RNA, ZG-O

Conflicts of Interest

Nothing to report.

References

1. Chang D, Nalls MA, Hallgrímsdóttir IB, et al. A meta-analysis of genome-wide association studies identifies 17 new Parkinson's disease risk loci. Nature genetics. 2017;49(10):1511.
2. Nalls MA, Pankratz N, Lill CM, et al. Large-scale meta-analysis of genome-wide association data identifies six new risk loci for Parkinson's disease. Nature genetics. 2014;46(9):989.
3. Cang C, Aranda K, Seo Y-j, Gasnier B, Ren D. TMEM175 is an organelle K+ channel regulating lysosomal function. Cell. 2015;162(5):1101-12.
4. Gan-Or Z, Dion PA, Rouleau GA. Genetic perspective on the role of the autophagy-lysosome pathway in Parkinson disease. Autophagy. 2015;11(9):1443-57.
5. Martini-Stoica H, Xu Y, Ballabio A, Zheng H. The autophagy–lysosomal pathway in neurodegeneration: a TFEB perspective. Trends in neurosciences. 2016;39(4):221-34.
6. Gan-Or Z, Amshalom I, Kilarski LL, et al. Differential effects of severe vs mild GBA mutations on Parkinson disease. Neurology. 2015 Mar 3;84(9):880-7.
7. Sidransky E, Nalls MA, Aasly JO, et al. Multicenter analysis of glucocerebrosidase mutations in Parkinson's disease. N Engl J Med. 2009 Oct 22;361(17):1651-61.
8. Jinn S, Drolet RE, Cramer PE, et al. TMEM175 deficiency impairs lysosomal and mitochondrial function and increases α-synuclein aggregation. Proceedings of the National Academy of Sciences. 2017:201616332.
9. Arnaldi D, Antelmi E, St Louis EK, Postuma RB, Arnulf I. Idiopathic REM sleep behavior disorder and neurodegenerative risk: To tell or not to tell to the patient? How to minimize the risk? Sleep Med Rev. 2017 Dec;36:82-95.
10. Fereshtehnejad SM, Postuma RB. Subtypes of Parkinson's Disease: What Do They Tell Us About Disease Progression? Curr Neurol Neurosci Rep. 2017 Apr;17(4):34.
11. Hughes AJ, Daniel SE, Kilford L, Lees AJ. Accuracy of clinical diagnosis of idiopathic Parkinson's disease: a clinico-pathological study of 100 cases. Journal of Neurology, Neurosurgery & Psychiatry. 1992;55(3):181-4.
12. O'Roak BJ, Vives L, Fu W, et al. Multiplex targeted sequencing identifies recurrently mutated genes in autism spectrum disorders. Science. 2012;338(6114):1619-22.

13. Ross JP, Dupre N, Dauvilliers Y, et al. Analysis of DNAJC13 mutations in French-Canadian/French cohort of Parkinson's disease. Neurobiology of aging. 2016;45:212. e13-. e17.
14. Li H, Durbin R. Fast and accurate short read alignment with Burrows–Wheeler transform. Bioinformatics. 2009;25(14):1754-60.
15. McKenna A, Hanna M, Banks E, et al. The Genome Analysis Toolkit: a MapReduce framework for analyzing next-generation DNA sequencing data. Genome research. 2010;20(9):1297-303.
16. Wang K, Li M, Hakonarson H. ANNOVAR: functional annotation of genetic variants from high-throughput sequencing data. Nucleic acids research. 2010;38(16):e164-e.
17. Lek M, Karczewski KJ, Minikel EV, et al. Analysis of protein-coding genetic variation in 60,706 humans. Nature. 2016;536(7616):285.
18. Lill CM, Roehr JT, McQueen MB, et al. Comprehensive research synopsis and systematic meta-analyses in Parkinson's disease genetics: The PDGene database. PLoS genetics. 2012;8(3):e1002548.
19. Olivova P, Cullen E, Titlow M, et al. An improved high-throughput dried blood spot screening method for Gaucher disease. Clin Chim Acta. 2008 Dec;398(1-2):163-4.
20. Reuser AJ, Verheijen FW, Bali D, et al. The use of dried blood spot samples in the diagnosis of lysosomal storage disorders--current status and perspectives. Mol Genet Metab. 2011 Sep-Oct;104(1-2):144-8.
21. Alcalay RN, Levy OA, Waters CH, et al. Glucocerebrosidase activity in Parkinson's disease with and without GBA mutations. Brain. 2015;138(9):2648-58.
22. Viechtbauer W. Conducting meta-analyses in R with the metafor package. J Stat Softw. 2010;36(3):1-48.
23. Purcell S, Neale B, Todd-Brown K, et al. PLINK: a tool set for whole-genome association and population-based linkage analyses. The American Journal of Human Genetics. 2007;81(3):559-75.
24. Rodrigues CH, Pires DE, Ascher DB. DynaMut: predicting the impact of mutations on protein conformation, flexibility and stability. Nucleic Acids Res. 2018 Jul 2;46(W1):W350-W5.
25. Webb B, Sali A. Comparative protein structure modeling using MODELLER. Current protocols in protein science. 2016;86(1):2.9. 1-2.9. 37.

26. Lee C, Guo J, Zeng W, et al. The lysosomal potassium channel TMEM175 adopts a novel tetrameric architecture. Nature. 2017;547(7664):472.
27. Wu S, Zhang Y. LOMETS: a local meta-threading-server for protein structure prediction. Nucleic acids research. 2007;35(10):3375-82.
28. Lomize MA, Lomize AL, Pogozheva ID, Mosberg HI. OPM: orientations of proteins in membranes database. Bioinformatics. 2006;22(5):623-5.
29. Jo S, Lim JB, Klauda JB, Im W. CHARMM-GUI Membrane Builder for mixed bilayers and its application to yeast membranes. Biophysical journal. 2009;97(1):50-8.
30. Huang J, MacKerell AD. CHARMM36 all-atom additive protein force field: Validation based on comparison to NMR data. Journal of computational chemistry. 2013;34(25):2135-45.
31. Jo S, Kim T, Im W. Automated builder and database of protein/membrane complexes for molecular dynamics simulations. PloS one. 2007;2(9):e880.
32. Phillips JC, Braun R, Wang W, et al. Scalable molecular dynamics with NAMD. Journal of computational chemistry. 2005;26(16):1781-802.
33. Feller SE, Zhang Y, Pastor RW, Brooks BR. Constant pressure molecular dynamics simulation: the Langevin piston method. The Journal of chemical physics. 1995;103(11):4613-21.
34. Martyna GJ, Tobias DJ, Klein ML. Constant pressure molecular dynamics algorithms. The Journal of Chemical Physics. 1994;101(5):4177-89.
35. Ryckaert J-P, Ciccotti G, Berendsen HJ. Numerical integration of the cartesian equations of motion of a system with constraints: molecular dynamics of n-alkanes. Journal of Computational Physics. 1977;23(3):327-41.
36. Essmann U, Perera L, Berkowitz ML, Darden T, Lee H, Pedersen LG. A smooth particle mesh Ewald method. The Journal of chemical physics. 1995;103(19):8577-93.
37. MacKerell Jr AD, Bashford D, Bellott M, et al. All-atom empirical potential for molecular modeling and dynamics studies of proteins. The journal of physical chemistry B. 1998;102(18):3586-616.
38. Lee BR, Kamitani T. Improved immunodetection of endogenous α-synuclein. PLoS one. 2011;6(8):e23939.

39. Gan-Or Z, Liong C, Alcalay RN. GBA-Associated Parkinson's Disease and Other Synucleinopathies. Curr Neurol Neurosci Rep. 2018 Jun 8;18(8):44.
40. Dumitriu A, Pacheco CD, Wilk JB, et al. Cyclin-G-associated kinase modifies α-synuclein expression levels and toxicity in Parkinson's disease: results from the GenePD Study. Human molecular genetics. 2011;20(8):1478-87.
41. Gan-Or Z, Mirelman A, Postuma RB, et al. GBA mutations are associated with Rapid Eye Movement Sleep Behavior Disorder. Ann Clin Transl Neurol. 2015 Sep;2(9):941-5.
42. Ouled Amar Bencheikh B, Ruskey JA, Arnulf I, et al. LRRK2 protective haplotype and full sequencing study in REM sleep behavior disorder. Parkinsonism Relat Disord. 2018 Jul;52:98-101.
43. Li J, Ruskey JA, Arnulf I, et al. Full sequencing and haplotype analysis of MAPT in Parkinson's disease and rapid eye movement sleep behavior disorder. Mov Disord. 2018 May 14.
44. Gan-Or Z, Montplaisir JY, Ross JP, et al. The dementia-associated APOE epsilon4 allele is not associated with rapid eye movement sleep behavior disorder. Neurobiol Aging. 2017 Jan;49:218 e13- e15.
45. Postuma RB, Gagnon J-F, Bertrand J-A, Marchand DG, Montplaisir JY. Parkinson risk in idiopathic REM sleep behavior disorder Preparing for neuroprotective trials. Neurology. 2015;84(11):1104-13.
46. Clare JJ. Targeting ion channels for drug discovery. Discovery medicine. 2010;9(46):253-60.
47. Sterea AM, Almasi S, El Hiani Y. The hidden potential of lysosomal ion channels: a new era of oncogenes. Cell calcium. 2018.
48. Murphy KE, Gysbers AM, Abbott SK, et al. Reduced glucocerebrosidase is associated with increased α-synuclein in sporadic Parkinson's disease. Brain. 2014;137(3):834-48.
49. Bae E-J, Yang N-Y, Song M, et al. Glucocerebrosidase depletion enhances cell-to-cell transmission of α-synuclein. Nature communications. 2014;5:4755.

Tables

Table 1. *TMEM175* coding variants associated with PD and RBD.

	p.M393T				p.Q65P			
Cohort	**Freq. Cases**	**Freq. Controls**	**OR (95% CI)**	**P value**	**Freq. Cases**	**Freq. Controls**	**OR (95% CI)**	**P value**
Parkinson Disease								
McGill	0.2104	0.1865	1.38 (1.07-1.79)	0.015	0.0971	0.1265	0.70 (0.51-0.97)	0.034
Columbia	0.2919	0.2287	1.44 (1.10-1.87)	0.008	0.0881	0.1175	0.73 (0.49-1.07)	0.106
Sheba	0.3433	0.2940	1.183 (0.80-1.76)	0.407	0.1114	0.1189	0.76 (0.4-1.44)	0.397
Meta-Analysis (PD)	-	-	1.37 (1.15-1.61)	0.0003	-	-	0.72 (0.57-0.91)	0. 005
REM Sleep Behavior Disorder								
McGill	0.2308	0.1874	1.59 (1.20-2.11)	0.001	0.1135	0.1269	0.88 (0.63-1.23)	0.45
Meta-Analysis (PD + RBD)	-	-	1.42 (1.23-1.64)	<0.0001	-	-	0.77 (0.63-0.93)	0. 0063

Freq, frequency; OR, odds ratio; CI, confidence interval; PD, Parkinson disease; REM, rapid eye movement; RBD, REM sleep behavior disorder.

Figure 1.

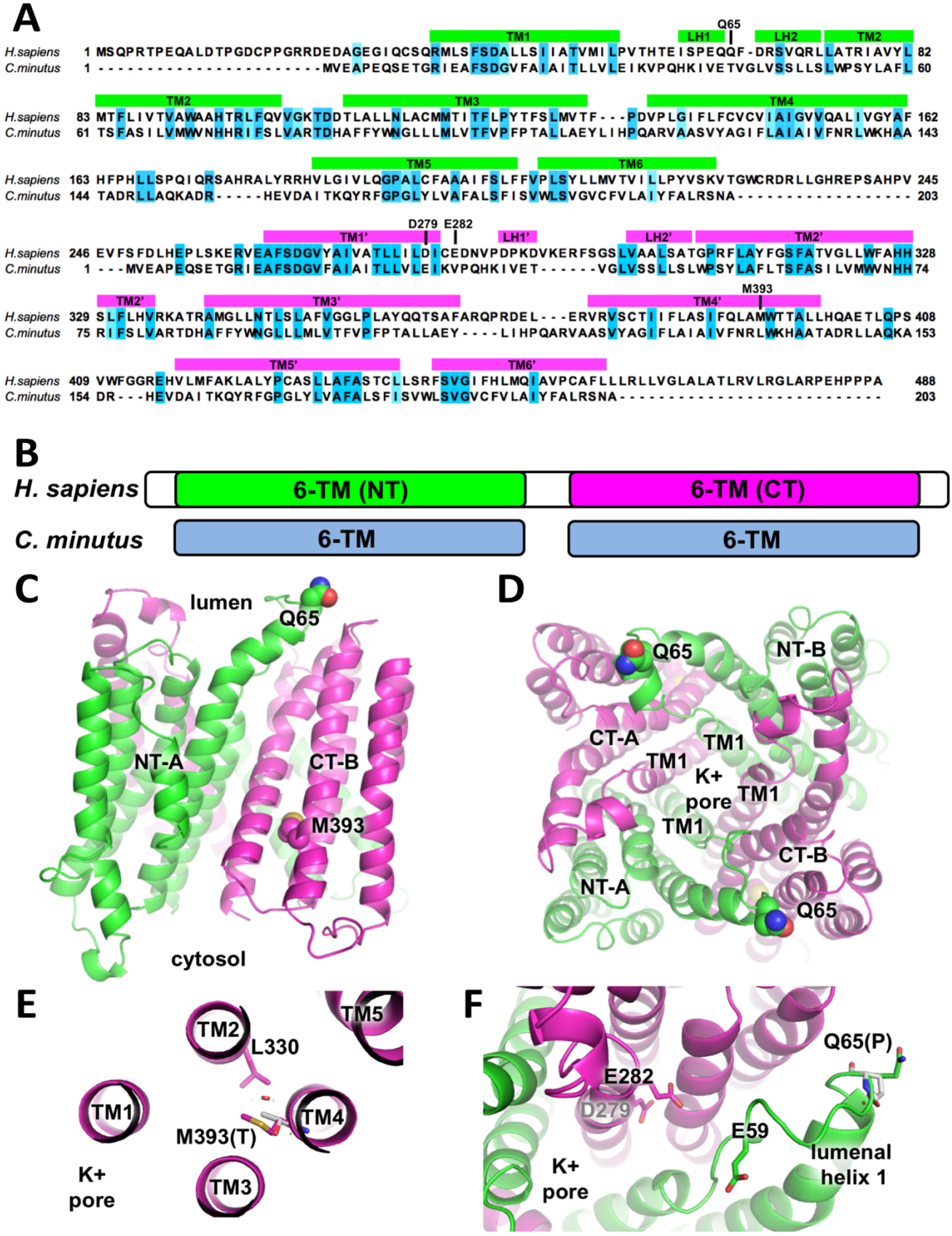
A
Q65
TM1
LH1
LH2
TM2
H.sapiens 1 MSQPRTPEQALDTPGDCPPGRRDEDAGEGIQCSQRMLSFSDALLSIIATVMILPVTHTEISPEQQF-DRSVQRLLATRIAVYL 82
C.minutus 1 ----------MVEAPEQSETGRIEAFSDGVFAIAITLLVLEIKVPQHKIVETVGLVSSLLSLWPSYLAFL 60
TM2
TM3
TM4
H.sapiens 83 MTFLIVTVAWAAHTRLFQVVGKTDDTLALLNLACMMTITFLPYTFSLMVTF---PDVPLGIFLFCVCVIAIGVVQALIVGYAF 162
C.minutus 61 TSFASILVMWVNHHRIFSLVARTDHAFFYWNGLLLMLVTFVPFPTALLAEYLIHPQARVAASVYAGIFLAIAIVFNRLWKHAA 143
TM5
TM6
H.sapiens 163 HFPHLLSPQIQRSAHRALYRRHVLGIVLQGPALCFAAAIFSLFFVPLSYLLMVTVILLPYVSKVTGWCRDRLLGHREPSAHPV 245
C.minutus 144 TADRLLAQKADR-----HEVDAITKQYRFGPGLYLVAFALSFISVWLSVGVCFVLAIYFALRSNA---------- 203
D279 E282
TM1'
LH1'
LH2'
TM2'
H.sapiens 246 EVFSFDLHEPLSKERVEAFSDGVYAIVATLLILDICEDNVPDPKDVKERFSGSLVAALSATGPRFLAYFGSFATVGLLWFAHH 328
C.minutus 1 ---MVEAPEQSETGRIEAFSDGVFAIAITLLVLEIKVPQHKIVET------VGLVSSLLSLWPSYLAFLTSFASILVMWVNHH 74
M393
TM2'
TM3'
TM4'
H.sapiens 329 SLFLHVRKATRAMGLLNTLSLAFVGGLPLAYQQTSAFARQPRDEL---ERVRVSCTIIFLASIFQLAMWTTALLHQAETLQPS 408
C.minutus 75 RIFSLVARTDHAFFYWNGLLLMLVTFVPFPTALLAEY----LIHPQARVAASVYAGIFLAIAIVFNRLWKHAATADRLLAQKA 153
TM5'
TM6'
H.sapiens 409 VWFGGREHVLMFAKLALYPCASLLAFASTCLLSRFSVGIFHLMQIAVPCAFLLLRLLVGLALATLRVLRGLARPEHPPPA 488
C.minutus 154 DR---HEVDAITKQYRFGPGLYLVAFALSFISVWLSVGVCFVLAIYFALRSNA---------- 203
B
H. sapiens
6-TM (NT)
6-TM (CT)
C. minutus
6-TM
6-TM
C
lumen
Q65
NT-A
CT-B
M393
cytosol
D
Q65
NT-B
CT-A
TM1
TM1
K+
pore
TM1
TM1
CT-B
NT-A
Q65
E
TM2
L330
TM5
TM1
TM4
M393(T)
K+
pore
TM3
F
Q65(P)
E282
D279
E59
lumenal
helix 1
K+
pore

Figure 2

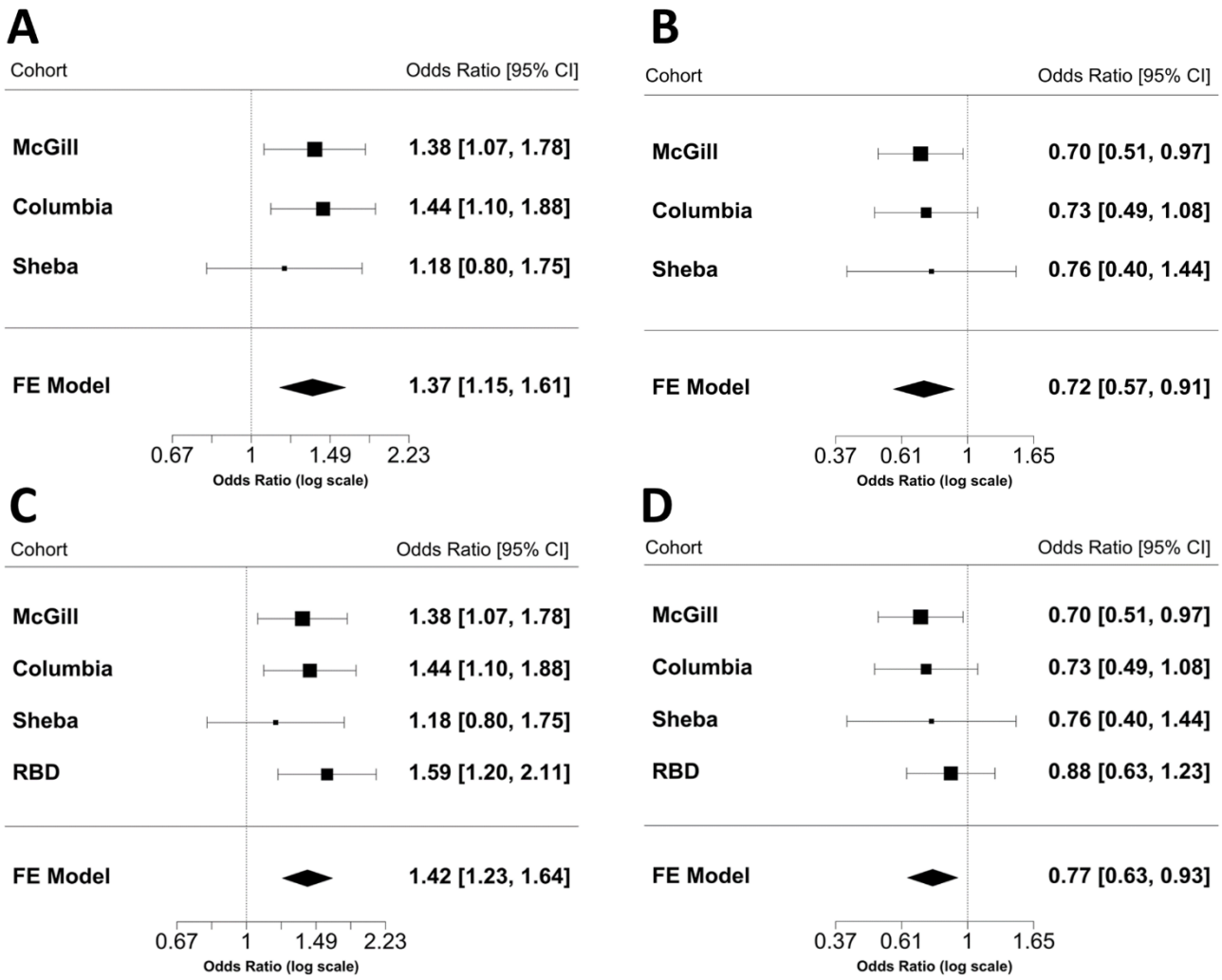
A
Cohort
Odds Ratio [95% CI]
McGill
1.38 [1.07, 1.78]
Columbia
1.44 [1.10, 1.88]
Sheba
1.18 [0.80, 1.75]
FE Model
1.37 [1.15, 1.61]
0.67
1
1.49
2.23
Odds Ratio (log scale)
B
Cohort
Odds Ratio [95% CI]
McGill
0.70 [0.51, 0.97]
Columbia
0.73 [0.49, 1.08]
Sheba
0.76 [0.40, 1.44]
FE Model
0.72 [0.57, 0.91]
0.37
0.61
1
1.65
Odds Ratio (log scale)
C
Cohort
Odds Ratio [95% CI]
McGill
1.38 [1.07, 1.78]
Columbia
1.44 [1.10, 1.88]
Sheba
1.18 [0.80, 1.75]
RBD
1.59 [1.20, 2.11]
FE Model
1.42 [1.23, 1.64]
0.67
1
1.49
2.23
Odds Ratio (log scale)
D
Cohort
Odds Ratio [95% CI]
McGill
0.70 [0.51, 0.97]
Columbia
0.73 [0.49, 1.08]
Sheba
0.76 [0.40, 1.44]
RBD
0.88 [0.63, 1.23]
FE Model
0.77 [0.63, 0.93]
0.37
0.61
1
1.65
Odds Ratio (log scale)

Figure 3.

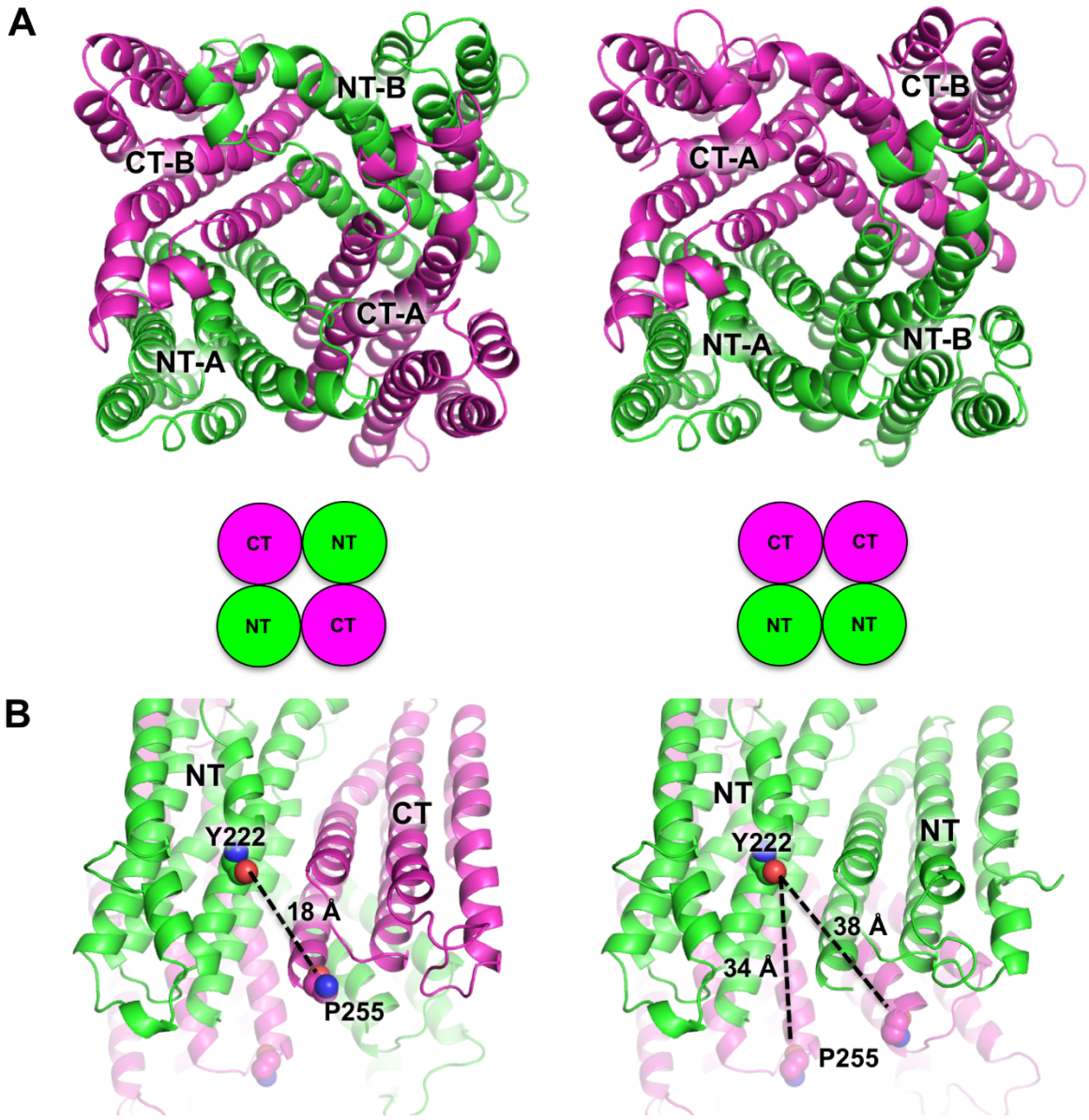
A
NT-B
CT-B
CT-A
NT-A
CT-B
CT-A
NT-A
NT-B
CT
NT
NT
CT
CT
CT
NT
NT
B
NT
Y222
CT
18 Å
P255
NT
Y222
NT
38 Å
34 Å
P255

Figure 4.

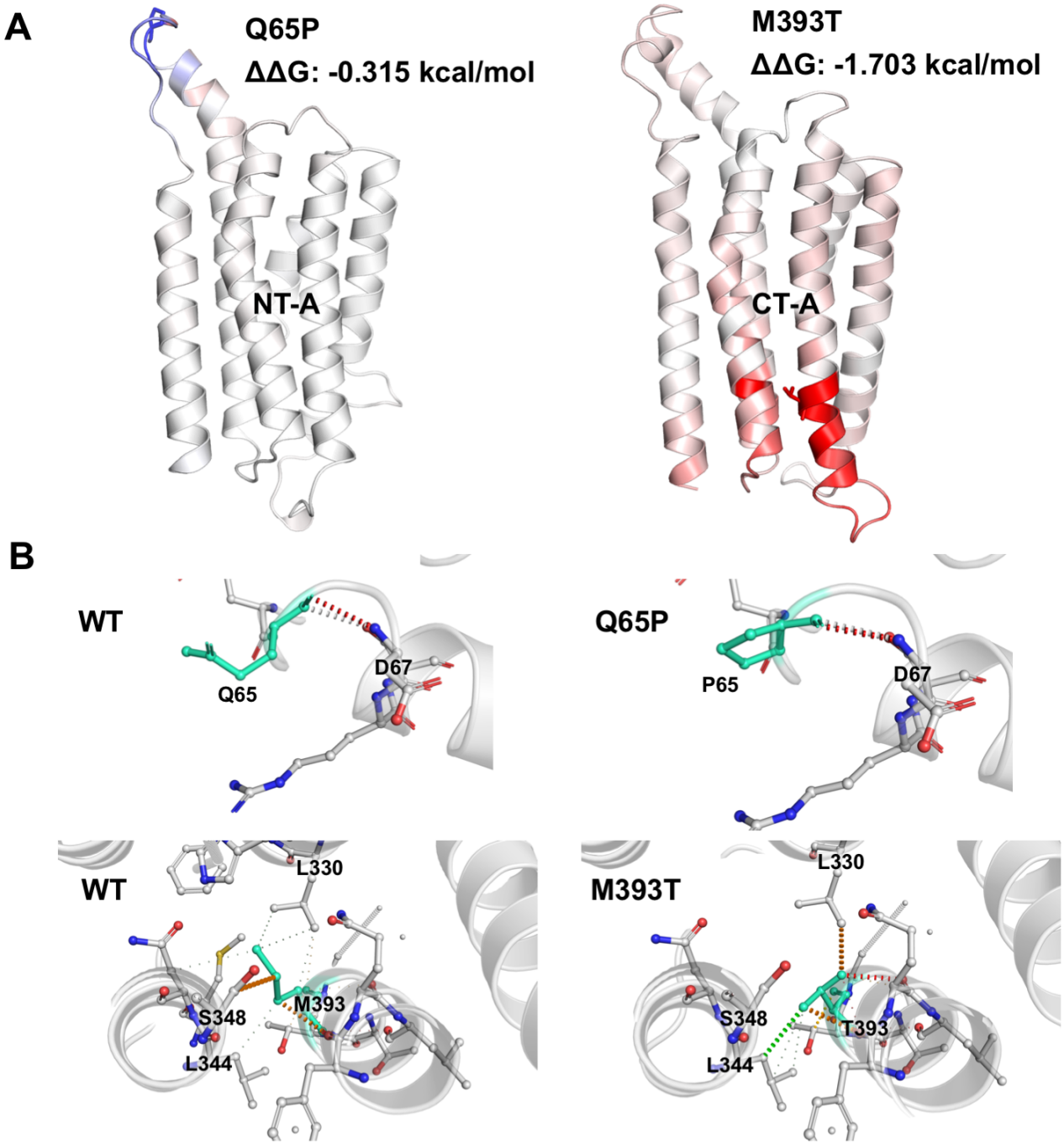
A
Q65P
ΔΔG: -0.315 kcal/mol
NT-A
M393T
ΔΔG: -1.703 kcal/mol
CT-A
B
WT
Q65
D67
Q65P
P65
D67
WT
L330
S348
M393
L344
M393T
L330
S348
T393
L344

Figure 5

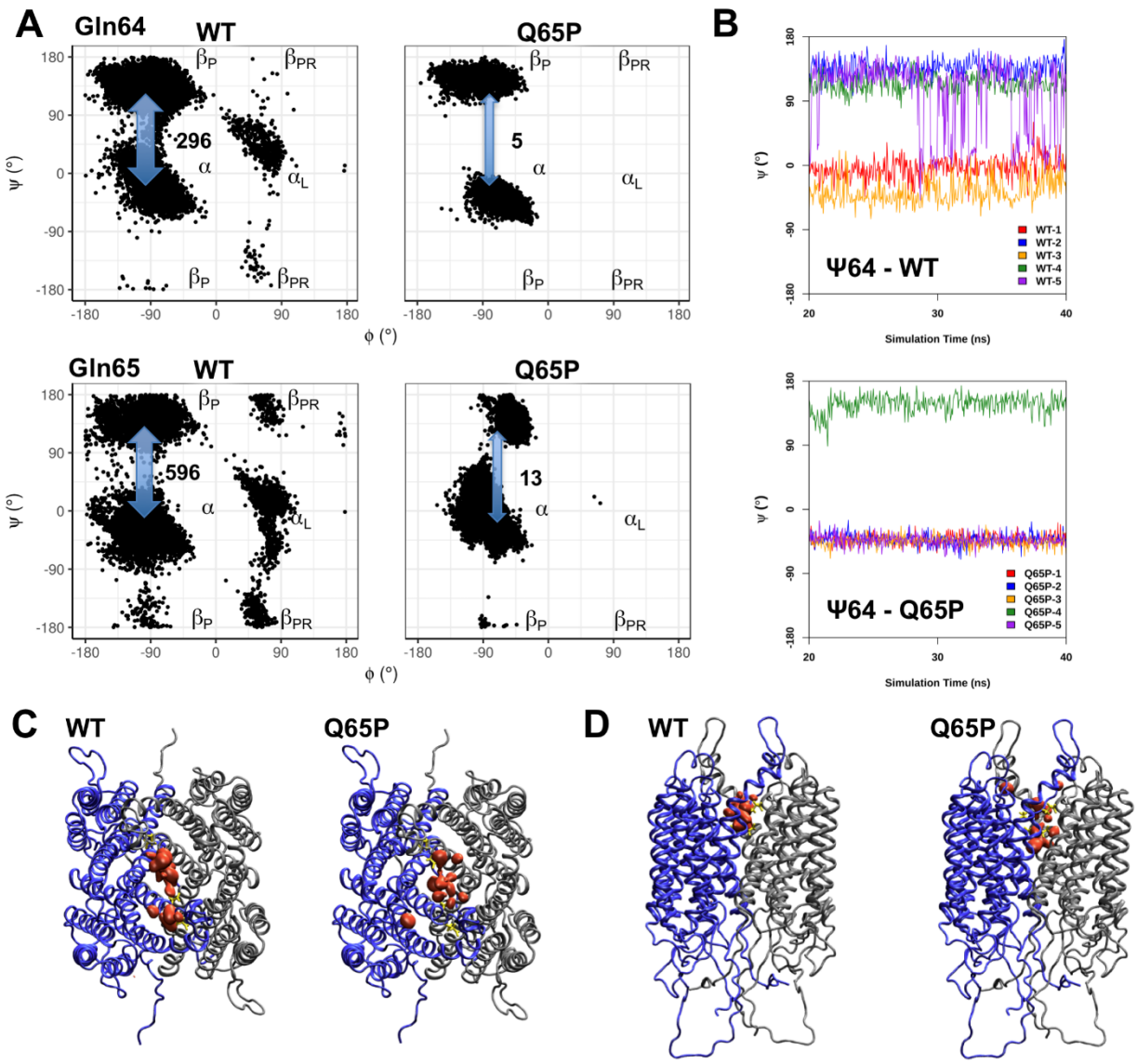
A
Gln64
WT
Q65P
Gln65
WT
Q65P
296
5
596
13
ψ (°)
ϕ (°)
B
Ψ64 - WT
Ψ64 - Q65P
WT-1
WT-2
WT-3
WT-4
WT-5
Q65P-1
Q65P-2
Q65P-3
Q65P-4
Q65P-5
Simulation Time (ns)
C
WT
Q65P
D
WT
Q65P

Figure 6

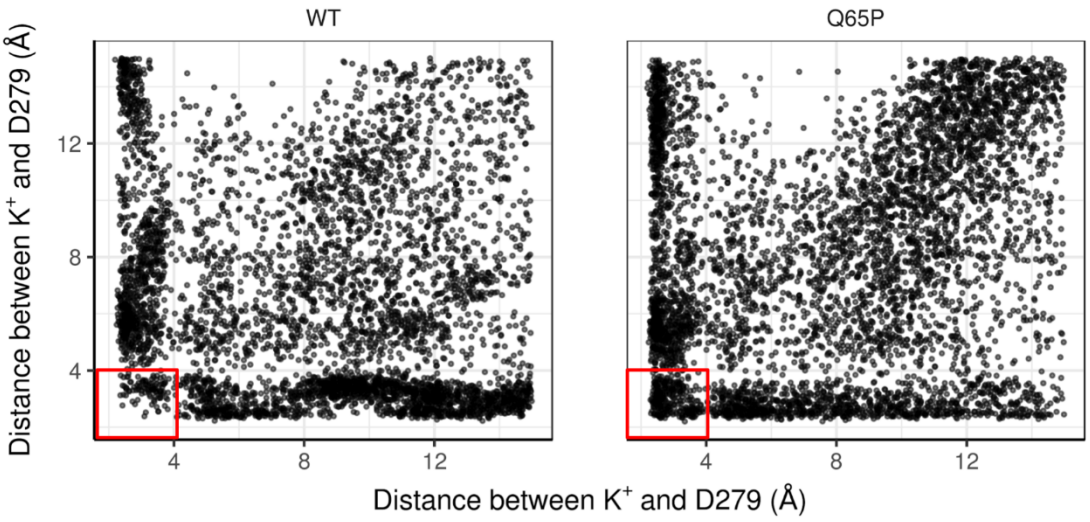
WT
Q65P
Distance between K+ and D279 (Å)
12
8
4
4
8
12
Distance between K+ and D279 (Å)

Figure 7.

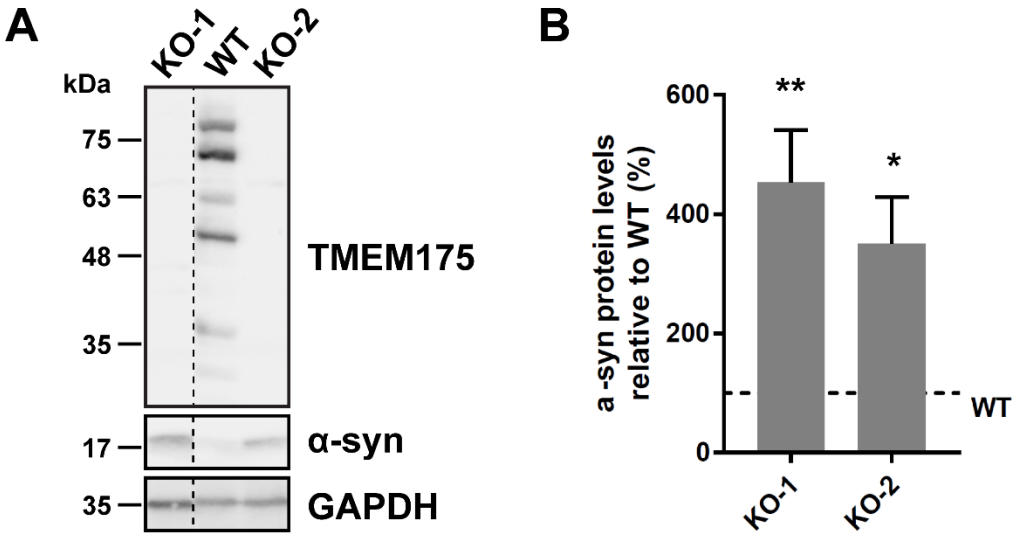
A
KO-1
WT
KO-2
kDa
75
63
48
35
TMEM175
17
α-syn
35
GAPDH
B
a -syn protein levels relative to WT (%)
600
400
200
0
**
*
WT
KO-1
KO-2

Figure legends

Figure 1. Homology model of human TMEM175. **(A)** Sequence alignment of TMEM175 orthologs from Homo sapiens and Chamaesiphon minutus. Transmembrane (TM) and lumenal (LH) helices are indicated as bars. Conserved residues are highlighted in blue. **(B)** Domain structure of human TMEM175, which of two 6-transmembrane domains in tandem, each showing homology to the C. minutus TMEM175 ortholog. **(C,D)** Side (C) and top (D) views of a hTMEM175 model, with the N- and C-terminal domains colored in green and magenta, respectively. The channel adopts a pseudo-tetrameric structure, with chains A/B assembling via symmetric, reciprocal interactions. The side-chains of Gln65 and Met393 are shown as spheres. **(E)** Close-up view of Met393, showing the impact of the p.M393T mutation in transmembrane helix 4 (TM4). The side-chain methyl of Thr393 (white) might clash with Leu330 in TM2, thus destabilizing the domain. **(F)** Close-up view of Gln65, showing the impact of the p.Q65P mutation. Pro65 (white) would introduce backbone clash in the loop following helix 1, forcing the backbone of this loop to adopt different dynamics. The side-chains of acidic residues along the pore that may contribute to K+ selectivity are shown as sticks.

Figure 2. Fixed-effect meta-analysis for pooled odds ratios of *TMEM175* variants in PD. **(A)** *TMEM175* variant p.M393T in the three PD cohorts (p=0.0003). **(B)** *TMEM175* variant p.Q65P in the three PD cohorts (p=0.005). **(C)** *TMEM175* p.M393T in the three PD cohorts combined with RBD (p<0.0001). **(D)** *TMEM175* p.Q65P in the three PD cohorts combined with RBD (p=0.0063).

Figure 3. Possible configurations for the pseudo-tetramer formed by human TMEM175. **(A)** Top view showing two possible configurations for the pseudo-tetramer formed by hTMEM175. **(B)** Cartoon showing how the linker between the N- and C-terminal domains crosses over the pore entrance in the model on the right.

Figure 4. Analysis of TMEM175 stability with DynaMut. **(A)** Changes in vibrational entropy energy between wild-type and mutants. Amino acids colored according to the vibrational entropy change upon mutation. Blue represents a rigidification of the structure and red a gain in flexibility. The predicted change in free energy is shown for each mutation. **(B)** Analysis of contact mediated by residues around mutation sites. Wild-type and mutant residues are colored in light-green and are also represented as sticks alongside with the surrounding residues which are involved on any type of interactions. H-bonds are shown in red, VdW contacts in grey, Hydrophobic-VdW clashes in green, and polar-VdW clashes in orange.

Figure 5. Molecular dynamics of human TMEM175 WT and Q65P variants. **(A)** Ramachandran plots of amino acids Gln64 and Gln/Pro65 in all models of the MD simulation for the WT and Q65P channels. (**B)** Trajectory of dihedral angles for one simulation of WT and Q65P models. Arrows indicate “flips” in the dihedral angle. **(C,D)** Top **(C)** and side **(D)** views of WT and Q65P channels, respectively. In both channels, subunits A (grey) and B (blue) are shown in cartoon representation. ASP 279 and GLU 282 residues enclosing the K+ binding pockets are shown as yellow licorice sticks. Red pockets indicate the regions in which high K+ density was observed.

Figure 6. Distance between K+ ions and the side-chains OD atoms of Asp279 in both WT and Q65P TMEM175 MD simulations. The number of dots in the x<4 & y<4 region (boxed in red) is 108 for WT, and 316 for Q65P, implying the two-side chains comes simultaneously in contact with K+.

Figure 7. *TMEM175* knock-out cells display increased α-syn levels. **(A)** Representative western blot analysis of TMEM175 KO cells lysates (two clones are shown, KO-1 and KO-2) showing loss of TMEM175 antibody reactive bands, and increased levels of α-synuclein. The dotted line indicates that the KO-1 lane is from the same gel and membrane as WT and KO-2. **(B)** Densitometric quantification of α-synuclein signal normalized to GAPDH (% of WT, WT levels are indicated by the dotted line). Mean ±SEM is shown. * $p<0.05$; ** $p<0.01$; Student's t-test ; n=4.